Delayed resonator with hybrid multiple-delayed control for enhanced complete vibration suppression

Yifan Liu, Bo Yan, Li Cheng

***Abstract*—Delayed resonator (DR) is an active vibration absorber that can enable complete vibration suppression of a force-excited primary structure at a given frequency by manipulating the loop delay. This work introduces a hybrid multiple-delayed control law to actuate the DR by incorporating the delayed states of the primary structure in addition to absorber states. The key benefit of this control law is its complete compliance with the tuning mechanism of the conventional absorber-based control parameters, thus simplifying implementation. Improved vibration suppression is sought in three aspects: 1). Shortened settling time of transient process; 2). Widened operable low-frequency band; and 3). Enhanced robustness against residual vibrations. Based on spectral analysis, stability analysis, and frequency response analysis, selection rules of the two newly introduced control parameters related to the primary structure, including a gain plus a delay, are established to maximize control performance. The resulting significantly enhanced vibration suppression is justified by comparisons with classical DRs.**

***Index Terms*—Active vibration control, Delayed resonator, Multiple-delayed system, Vibration absorber.**

I. Introduction

SINCE ince the invention of vibration absorbers by Frahm [1] in the 1900s, this efficient vibration reduction technique has been widely applied in fields such as mechanical, civil, and aerospace engineering, with various modifications reported to improve vibration suppression efficacy [2]. This work focuses on the concept of delayed resonator (DR) proposed by Olgac and Holm-Hansen [3], which enables complete vibration suppression at a given frequency by actuating the absorber following an actively delayed control law. The manipulation of delay makes DR a typical counter-intuitive example that larger delays can enhance control performance. Besides, taking delay as a control parameter endows a single control term with additional tuning freedom while keeping system linearity, and it reduces the number of required feedback states compared with the classical PD control by tuning delay to alter state phases, thus enhancing robustness [4]. Furthermore, the feedback states to achieve the DR scheme are not limited to displacement [3] and velocity [5], it also can be acceleration [6], which facilitates practical implementations.

Research on DR has been prosperous. Focusing on the past decade, Xu and Sun [7] identified and prolonged the loop delay of an active vibration absorber, resulting in better vibration suppression performance. Eris et al. [8] additionally injected a non-delayed term into the control law, which was then optimized to expedite responses. Zhang et al. [9] modeled friction effects when tuning the DR and showed that excitation can affect system stability if friction is non-negligible. To reduce noise effects when collecting feedback states, Pilbauer et al. [10], Kučera et al. [11], and Liu et al. [12] adopted distributed-delayed control laws so that actuation forces depend on the sum of all the feedback states sampled within a designated past time interval. Besides, Vyhlídal et al. [13] summarized the tuning mechanisms of the DR when incorporating different feedback states and evaluated the residual vibrations caused by the mismatch between the actual vibration frequency and the detected one, see also [14], [15] for handling such residual vibrations. Subsequently, Cai et al. [16] established the relationship between the tuning mechanisms regarding different system states using fractional-order operators. Utilizing the transcendentality caused by delay, Valášek et al. [17] assigned multiple pairs of imaginary roots to the DR subsystem to suppress multiple-frequency vibration. Moreover, the DR structure was modified to seek mechanical advantage. For instance, a lever-type DR was reported in [18] to reduce residual vibrations while compressing absorber strokes. A high-static-low-dynamic-stiffness DR was proposed in [19] to enhance low-frequency performance by reducing the absorber natural frequency without compromising supporting capacity. The DR of multiple degrees of freedom (MDOF) was also considered to achieve the non-collected vibration suppression [20]–[23], i.e., the point to achieve complete vibration suppression can differ from the point where feedback forces are applied. In addition to complete vibration suppression, delayed control has also been widely applied for vibration reduction [24]–[27].

We notice that one key index to improve the performance of DR is to reduce the transient process when settling the primary structure, as reported in [8], [12], [14], [16]. The method is straightforward by optimizing control parameters to place the dominant (i.e., the rightmost) characteristic roots of the system leftmost. However, control laws of previous works were mainly based on absorber states, making such optimization an 'indirect' approach to expedite the final objective to suppress the vibrations on the primary. Given that absorber states are necessary to dictate feedback actuation to help neutralize forces on the primary for complete vibration suppression in steady states since feedback forces depending on a completely settled primary structure are zero, we adopt a hybrid control law that combines the states of both the absorber and the primary. By doing so, the additional feedback forces related to the primary take effect only in the transient

Manuscript received September 24, 2025; revised December 29, 2024. This work was supported in part by National Natural Science Foundation of China under grant nos. 52422504 and 52175125. (Corresponding author: Li Cheng).

Yifan Liu and Li Cheng are with the Department of Mechanical Engineering, The Hong Kong Polytechnic University, Hong Kong, China. (e-mail: liuyifan.hi@outlook.com; li.cheng@polyu.edu.hk).

Bo Yan is with the School of Mechanical Engineering, Zhejiang Sci-Tech University, Hangzhou, China (e-mail: yanbo@zstu.edu.cn).

0000–0000/00$00.00 © 2021 IEEE

process thus unaffecting the dominance of those related to the absorber in achieving complete vibration suppression in steady states, i.e., the additional forces do not affect the tuning mechanism of the conventional absorber-based feedback forces, yielding the so-called complete compliance. Notably, a similar control law was reported in [28] to enhance vibration isolation. While the system and control objectives of [28] were different from this work, it was found that introducing and manipulating the delays in such additional control forces can be beneficial. Hence, the states of the primary structure are additionally delayed to help expedite settling the primary itself, an interesting topic that seems contradictory. Similar to the DR, such an additional delay does not increase the number of control terms. Finally, a hybrid multiple-delayed control law is proposed and investigated.

In addition to the original motivations to expedite the transient process, we also seek the possible benefits of such a hybrid control law in two other key indices that are commonly used to evaluate the DR performance. The first is the width of the operable frequency band for complete vibration suppression. This issue has been mentioned in [12], [13], [16], showing that theoretically, no upper bounds exist, while lower bounds always exist due to stability issues, regardless of the feedback states used. The second one is the robustness in suppressing residual vibrations. The main factors causing residual vibrations can be noises and the inaccuracy in implementing control parameters that may stem from the aforementioned mismatch between the detected excitation frequency and the actual one. Solutions for this have been reported in [14], [15], [18], which, however, require advanced control laws or structural alterations that may be unconducive to implementation and stability. Alternatively, the proposed hybrid control law offers an easier solution thanks to the aforementioned complete compliance. Note that the common ground for enhancing such two indices (i.e., stability for the first index and smaller residual vibrations for the other) is that the primary exhibits oscillations once undesired consequences occur, making the newly introduced additional feedback forces related to the states of the primary nonzero for resistance. Overall, our contributions are twofold:

1) We proposed a novel hybrid multiple-delayed control law of complete compliance by additionally incorporating the delayed states of the primary into the feedback loop.
2) Based on spectral analysis, stability analysis, and frequency response analysis, we established a tuning framework for the new hybrid control law to maximize control performance in three commonly considered aspects.

The paper is structured as follows. Section II proposes the hybrid multiple-delayed control law. Spectral analyses to expedite transient process are conducted in Section III. Section IV extends the operable low-frequency band based on stability analysis. Section V shows how the hybrid control law can help suppress residual vibrations. The observed theoretical benefits are both numerically and experimentally verified in Section VI. Conclusions are drawn in Section VII. Italic symbols without the bar superscript '$\overline{\square}$' are dimensionless throughout the text.

II. Preliminaries

A common operating mode of the delayed resonator (DR) [3] is shown in Fig. 1(a), where a force feedback actuator $\bar{u}$ is injected into a vibration absorber substructure to enhance the settling of the primary structure harmonically excited by $\bar{f}_e$. The coupling dynamics between the slides and sliding bearings are modeled by a pair of stiffness and damping. Notably, such dynamics with the primary structure are incorporated into the stiffness $\bar{k}_p$ and damping $\bar{c}_p$, and the stiffness between the absorber and slides is ignored due to its small values compared with the mechanical spring $\bar{k}_a$. The aim is to completely settle the primary structure by properly tuning $\bar{u}$. The system behaves like Fig. 1(b) when the aim is achieved (i.e., $\left(\bar{c}_p, \bar{k}_p\right)$ take no dynamical effect), yielding the so-called complete vibration suppression.

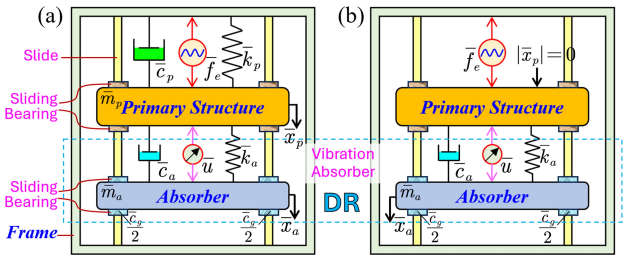

Fig. 1. (a). A common operating mode of the DR for settling force-excited primary structure. (b). Equivalent model of (a) when complete vibration suppression is achieved.

A. System modeling and the DR concept

Dynamics of the 2DOF system in Fig. 1(a), consisting of a primary structure and an absorber, are governed by

$$\begin{cases} \bar{m}_a\ddot{\bar{x}}_a + \bar{c}_g\dot{\bar{x}}_a + \bar{c}_a\left(\dot{\bar{x}}_a - \dot{\bar{x}}_p\right) + \bar{k}_a\left(\bar{x}_a - \bar{x}_p\right) = \bar{u}, \\ \bar{m}_p\ddot{\bar{x}}_p + \bar{c}_p\dot{\bar{x}}_p + \bar{k}_p\bar{x}_p + \bar{c}_a\left(\dot{\bar{x}}_a - \dot{\bar{x}}_a\right) + \bar{k}_a\left(\bar{x}_p - \bar{x}_a\right) = \bar{f}_e - \bar{u}, \end{cases} \tag{1}$$

where the subscripts $(\cdot)_p$ and $(\cdot)_a$ denote the primary structure and absorber, respectively; and notations $\bar{x}_{(\cdot)}$, $\bar{m}_{(\cdot)}$, $\bar{c}_{(\cdot)}$, and $\bar{k}_{(\cdot)}$ represent displacement, mass, damping, and stiffness, respectively. Moreover, $\bar{x}_{(\cdot)}$, $\bar{u}$, and $\bar{f}_e$ are all functions of the time $\bar{t}$. The desired complete vibration suppression requires $|\bar{x}_p| = 0$ when $\bar{f}_e \neq 0$. Substituting $|\bar{x}_p| = 0$ into (1) yields

$$\begin{cases} \bar{m}_a\ddot{\bar{x}}_a + \left(\bar{c}_a + \bar{c}_g\right)\dot{\bar{x}}_a + \bar{k}_a\bar{x}_a = \bar{u}, \\ -\bar{c}_a\dot{\bar{x}}_a - \bar{k}_a\bar{x}_a = \bar{f}_e - \bar{u}. \end{cases} \tag{2}$$

The first equation in (2) depicts the absorber dynamics in Fig. 1(b), and the second one means that the total forces by the damper $\bar{c}_a$, spring $\bar{k}_a$, and the counter force of $\bar{u}$ neutralize the excitation force $\bar{f}_e$, an evident prerequisite for $|\bar{x}_p| = 0$ when $\bar{f}_e \neq 0$. Following the DR prototype [3], we consider the absorber displacement-based control law for comparisons

$$\bar{u}_a\left(\bar{t}\right) = \bar{g}\bar{x}_a\left(\bar{t} - \bar{\tau}_a\right), \tag{3}$$

where $\bar{g}$ is the feedback gain and $\bar{\tau}_a$ is the time delay, two control parameters. Plugging (3) into the first equation in (2) and applying Laplace transform to the result lead to

$$\left(\bar{m}_a\bar{s}^2 + \left(\bar{c}_a + \bar{c}_g\right)\bar{s} + \bar{k}_a\right)X_a = \bar{g}e^{-\bar{\tau}\bar{s}}X_a, \tag{4}$$

where $\bar{s}$ is the Laplace variable, and $X_a = \mathscr{L}(\bar{x}_a)$, with $\mathscr{L}(\cdot)$ denoting the Laplace transform. Given the second equation in (2), $(\bar{x}_a, \bar{u}_a)$ are at the same frequency as that of $\bar{f}_e$, say $\bar{\omega}$. Substituting $\bar{s} = j\bar{\omega}$, $j = \sqrt{-1}$ into (4) yields

$$\bar{k}_a - \bar{m}_a\bar{\omega}^2 + j(\bar{c}_a + \bar{c}_g)\bar{\omega} = \bar{g}e^{-j\bar{\tau}\bar{\omega}}. \tag{5}$$

The equality conditions of the amplitude and argument of the two sides of (5) lead to the tuned pair of $(\bar{g}, \bar{\tau})$,

$$\begin{cases} \bar{g}_t(\bar{\omega}) = \pm\sqrt{\left(\bar{k}_a - \bar{m}_a\bar{\omega}^2\right)^2 + \left[(\bar{c}_a + \bar{c}_g)\bar{\omega}\right]^2}, \\ \bar{\tau}_{a,t,b}(\bar{\omega}) = \frac{1}{\bar{\omega}}\left[\mathrm{a\,tan}\left(\frac{-(\bar{c}_a+\bar{c}_g)\bar{\omega}}{\bar{k}_a - \bar{m}_a\bar{\omega}^2}\right) + 2\pi(b-1) + \rho\pi\right], \end{cases} \tag{6}$$

where $(\cdot)_t$ means 'tuned', $\rho = 0$ and $\rho = 1$ correspond to $g_t > 0$ and $g_t < 0$, respectively, and $b \in \mathbb{Z}^+$ is called branch number signifying the multiple-valued feature of the tuned delay, the mechanism of which can be referred to [3].

B. Hybrid multiple-delayed control law

One cannot manipulate the transient (or convergence) process if the DR is only tuned as per $(\bar{g}_t, \bar{\tau}_{a,t})$, given that $(\bar{g}_t, \bar{\tau}_{a,t})$ are completely governed by Fig. 1(b), which depicts system dynamics in steady states $|\bar{x}_p| = 0$. To expedite this process, we additionally consider the states of the primary structure when tuning the DR, yielding

$$\bar{u}_{ap}(\bar{t}) = \bar{g}\left[\bar{x}_a(\bar{t} - \bar{\tau}_a) + \beta\bar{x}_p(\bar{t} - \bar{\tau}_p)\right], \tag{7}$$

where β is a weight coefficient, and $\bar{\tau}_p$ is the time delay originating from twofold aspects similar to $\bar{\tau}_a$, i.e., 1). Inherent loop delays due to causality; 2). Artificially introduced delay as a control parameter to seek possible enhanced system performance by altering the state phase. We point out the control law $\bar{u}_{ap}$ is inspired by [28], while it is adopted here for different objectives and is investigated in different aspects. Next, we separate (7) as

$$\bar{u}_{ap}(\bar{t}) = \bar{u}_a(\bar{t}) + \bar{u}_p(\bar{t}), \tag{8}$$

where $\bar{u}_p = \beta\bar{g}\bar{x}_p(\bar{t} - \bar{\tau}_p)$. Clearly, $\bar{u}_p \neq 0$ when $\bar{x}_p \neq 0$, so properly tuning $(\beta, \bar{\tau}_p)$ helps expedite convergence to $|\bar{x}_p| = 0$. Note that the new control term $\bar{u}_p$ does not affect the control robustness (related to the number of control terms) of the desired complete vibration suppression in steady states since $|\bar{u}_p| = 0$ when $|\bar{x}_p| = 0$. Plugging $\bar{u} = \bar{u}_{ap}$ into (1) and performing the transformations

$$\begin{aligned} &\bar{\omega}_p = \sqrt{\bar{k}_p/\bar{m}_p}, \bar{\omega}_a = \sqrt{\bar{k}_a/\bar{m}_a}, \zeta_p = \frac{\bar{c}_p}{2\bar{m}_p\bar{\omega}_p}, \zeta_a = \frac{\bar{c}_a}{2\bar{m}_a\bar{\omega}_a}, \\ &\zeta_g = \frac{\bar{c}_g}{2\bar{m}_a\bar{\omega}_a}, \mu = \frac{\bar{m}_a}{\bar{m}_p}, v = \bar{\omega}_a/\bar{\omega}_p, x_a = \bar{x}_a/\bar{l}, x_p = \bar{x}_p/\bar{l}, \\ &t = \bar{t}\bar{\omega}_p, f_e = \frac{\bar{f}_e}{\bar{k}_p\bar{l}}, u_a = \frac{\bar{u}_a}{\bar{k}_p\bar{l}}, u_p = \frac{\bar{u}_p}{\bar{k}_p\bar{l}}, \omega = \frac{\bar{\omega}}{\bar{\omega}_p}, \end{aligned} \tag{9}$$

in which $\bar{l}$ denotes the unit length, yield the dimensionless governing equations

$$\begin{cases} \mu\left[\ddot{x}_a + 2\zeta_g v\dot{x}_a + 2\zeta_a v(\dot{x}_a - \dot{x}_p) + v^2(x_a - x_p)\right] \\ = g\left[x_a(t - \tau_a) + \beta x_p(t - \tau_p)\right], \\ \ddot{x}_p + 2\zeta_p\dot{x}_p + x_p + 2\mu v\left[\zeta_a(\dot{x}_p - \dot{x}_a) + v(x_p - x_a)\right] \\ = f_e - g\left[x_a(t - \tau_a) + \beta x_p(t - \tau_p)\right], \end{cases} \tag{10}$$

where $g = \bar{g}/\bar{k}_p$, $\tau_a = \bar{\tau}_a\bar{\omega}_p$, and $\tau_p = \bar{\tau}_p\bar{\omega}_p$. Remarkably, since the tuning is based on $|\bar{x}_p| = 0$, the control law $\bar{u}_{ap}$ follows the tuning mechanism of $(\bar{g}_t, \bar{\tau}_{a,t})$, regardless of $(\beta, \bar{\tau}_p)$. Accordingly, the dimensionless tuned pair is

$$\begin{cases} g_t(\omega) = \pm\mu\sqrt{\left(v^2 - \omega^2\right)^2 + 4v^2\omega^2(\zeta_a + \zeta_g)^2}, \\ \tau_{a,t,b}(\omega) = \frac{1}{\omega}\left[\mathrm{a\,tan}\left(\frac{-2(\zeta_a+\zeta_g)v\omega}{v^2-\omega^2}\right) + 2\pi(b-1) + \rho\pi\right]. \end{cases} \tag{11}$$

For discrimination, we hereafter call the DR actuated by u_a and the hybrid control law u_{ap} as the A-DR and the AP-DR, respectively. The benefits of the new AP-DR over the conventional A-DR, including the original motivation for expediting the transient process and two other key indices for bettering vibration suppression, are justified by comparisons.

III. Spectral Optimization

For linear systems, the duration of the transient process is dictated by the dominant (i.e., the rightmost) characteristic roots. Hence, the spectral distributions of the coupled system with respect to the variations of (β, τ_p) are investigated.

A. Characteristic equation and restrictions

Applying the Laplace transform to (10) yields

$$\mathbf{Z}(s)\mathbf{X} = \mathbf{F}, \tag{12}$$

where $\mathbf{X} = [X_a, X_p]^{\mathrm{T}}, \mathbf{F} = [0, F]^{\mathrm{T}}$, in which $X_p = \mathscr{L}(x_p)$ and $F = \mathscr{L}(f_e)$. Besides, one has

$$\mathbf{Z}(s) = \begin{bmatrix} z_{11}(s) & z_{12}(s) \\ z_{21}(s) & z_{22}(s) \end{bmatrix}, \tag{13}$$

where $s = \bar{s}/\bar{\omega}_p$, $z_{11} = \mu\left(s^2 + 2(\zeta_a + \zeta_g)vs + v^2\right) - ge^{-\tau_a s}$, $z_{12} = -\mu v(2\zeta_a s + v) - g\beta e^{-\tau_p s}$, $z_{22} = -\mu v(2\zeta_a s + v) + ge^{-\tau_a s}$, and $z_{22} = s^2 + 2\zeta_p s + 1 + \mu v(2\zeta_a s + v) + g\beta e^{-\tau_p s}$. The characteristic equation is then

$$\begin{aligned} &CE(s, g, \tau_a, \beta, \tau_p) = |\mathbf{Z}(s)| \\ &= \alpha_1(s)U_a(s) + \alpha_2(s)U_p(s) + \alpha_3(s) = 0, \end{aligned} \tag{14}$$

where $U_a = ge^{-\tau_a s}$, $U_p = g\beta e^{-\tau_p s}$, and $(\alpha_1, \alpha_2, \alpha_3)$ are polynomial coefficients in s. Clearly, the dominant roots of Eq. (14) must lie on the left half of the complex plane for stability, forming the basic restriction for selecting (β, τ_p). Denoting the upper bound of the allowed feedback actuation amplitude as $\bar{u}_{\max}$, we have $|\bar{g}_t|\left(|\bar{x}_a|_{\max} + |\beta|\,|\bar{x}_p|_{\max}\right) < \bar{u}_{\max}$, or,

$$|\beta| < \frac{1}{|\bar{x}_p|_{\max}}\left(\frac{\bar{u}_{\max}}{|\bar{g}_t(\omega)|} - |\bar{x}_a|_{\max}\right). \tag{15}$$

For safety concerns, $|\bar{x}_a|_{\max}$ can selected as the maximum stroke of the actuator $\bar{u}$, and $|\bar{x}_p|_{\max}$ can be taken as the motion amplitude of the primary structure when $\bar{u} = 0$. In our cases, $|\beta| < 10$ is considered. Note that introducing an upper bound of β also limits the consequences of destabilization.

B. Spectral analysis at a specific frequency

From Eqs. (11), (13) and (14), although the two newly introduced control parameters (β, τ_p) do not affect the tuning mechanism of (g, τ_a), they appear in the characteristic equation, thus affecting the spectral distribution and thus the transient process. Denoting the dominant root of Eq. (14) as $s_{dom} = \sigma + j\varpi$, the duration of the transient process, signified by 98% amplitude reduction, i.e., $e^{\sigma t} < 0.02$, can be estimated by $t_s = -4/\sigma, \sigma < 0$. Clearly, a smaller σ is preferred. We next consider an example system governed by

$$\begin{aligned} &\mu = 0.5285, v = 0.9862, \zeta_a = 0.1097, \zeta_g = 0.051, \\ &\zeta_p = 0.0665, \bar{\omega}_p = 38.96\text{rad/s}, \bar{\omega}_a = 38.42\text{rad/s}, \end{aligned} \tag{16}$$

and the related experimental setup are introduced in Section VI. Here, (β, τ_p) are expected to expedite the complete vibration suppression at $\bar{\omega} = 8$Hz (or $\omega = 1.2901$) for instance. Given that a smaller tuned delay enhances robustness against frequency variations [13], we adopt the tuned pairs at the first branch $b = 1$, yielding $(g_t, \tau_{a,t,1}) = (-0.4247, 0.4139)$ and $(g_t, \tau_{a,t,1}) = (0.4247, 2.8491)$. Differences between such two tuned delays, stemming from the half-cycle shift, can be used to alter the delay when it is too small to be implemented [13]. Since no analytical solutions exist for the spectrum of (14) due to transcendentality, we apply the QPmR algorithm [29], yielding the variations of σ with respect to (β, τ_p) in Fig. 2.

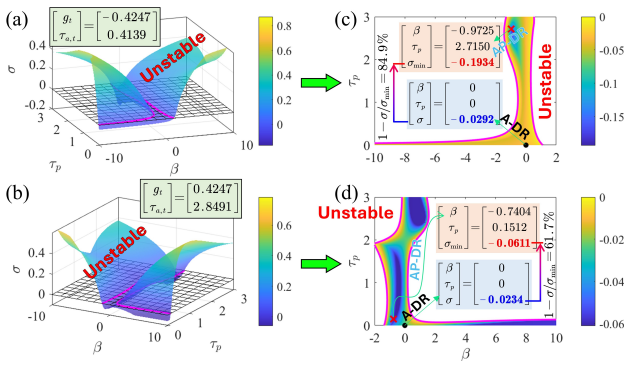

Fig. 2. (a, b). Variations of the real parts σ of the dominant roots of Eq. (14) with respect to (β, τ_p) when (g, τ) is tuned at $\bar{\omega} = 8$Hz. Girds denote $\sigma = 0$. (c) and (d) are zoomed plots of (a) and (b), respectively.

We can first find from Fig. 2(a, b) that the unstable regions signified by $\sigma > 0$ significantly vary as (β, τ_p) vary, so the additional control term u_p can significantly affect system stability. Furthermore, stability issues become more critical with extending unstable regions of (β, τ_p) when $g_t\beta < 0$ and when τ_p is large, agreeing with the practice. A large τ_p means that u_p mismatches the current states of the primary structure, which is further deteriorated by the reversed polarity $g_t\beta < 0$. Note that the system is unstable once $g_t\beta < 0$ is less than a negative threshold value even if $\tau_p = 0$.

For the desired expedited transient process, we focus on Fig. 2(c, d), where only the pairs (β, τ_p) rendering $\sigma < 0$ are shown. Compared with the conventional A-DR with $\beta = 0$, the AP-DR can manipulate the distributions of the dominant roots by tuning (β, τ_p). By comparing σ, the transient process of the A-DR at the given frequency can be expedited by up to 84.9% and 61.7% when $g_t < 0$ and $g_t > 0$, respectively. Counter-intuitively, such expedience may correspond to a large τ_p (for $g_t < 0$) and to $g_t\beta < 0$ (for $g_t > 0$), which can shrink the operable regions of (β, τ_p) due to stability issues, as aforementioned. The benefits of τ_p can also be found. First, by properly tuning τ_p, $|\beta|$ does not need to be sufficiently large to minimize σ, which helps reduce the peak instantaneous power of the feedback actuator, see also (15). Second, the introduction of τ_p improves the performance of the AP-DR that only tunes β. Note from Fig. 2(b, d) increasing $|\beta|$ when $\tau_p = 0$ can even prolong the transient process by raising σ, another counter-intuitive observation indicating that processing the latest information on the primary structure can be undesired for expediting settling the primary.

C. More general cases

Following Fig. 2, we next consider the performance of AP-DR in more general cases. By sweeping $\bar{\omega} \in [5\text{Hz}, 10\text{Hz}]$ at the step of 0.5Hz, we obtain the tuned pairs $(g_t, \tau_{a,t})$ shown in Fig. 3(a). For the AP-DR, the effects of (β, τ_p) on the minimum of σ, i.e., $\sigma_{\min}$, and accordingly, on the actual settling time $\bar{t}_s = t_s/\bar{\omega}_p$ are evaluated in Fig. 3(b, c).

Let us first focus on Fig. 3(b) for the cases $g_t < 0$. Given the previously revealed significant effects of τ_p on the optimum β to achieve $\sigma_{\min}$, we divide the interval of β into small and large $|\beta|$ cases depending on the threshold value $|\beta| = 2.5$, as signified in Fig. 3(b.1). Combining with Fig. 3(b.2), smaller amplitudes $|\beta|$ correspond to larger delays τ_p and vice versa, concurring with Fig. 2(b). The resulting variations of $\sigma_{\min}$ are shown in Fig. 3(b.3), where the preferred smaller $\sigma_{\min}$ values appear in small $|\beta|$ cases, a favorable condition to maximize the performance of the AP-DR in practice, especially considering that the optimum τ_p must be sufficiently small if $|\beta|$ is large, see Fig. 3(b.2). Once again, it signifies the aforementioned benefits of introducing and manipulating τ_p for limiting the amplitude $|\beta|$. We can also obtain similar conclusions in the cases $g_t > 0$, as shown in Fig. 3(c), except that smaller $\sigma_{\min}$ values around $\bar{\omega} = 7$Hz correspond to a large $|\beta|$, a trade-off needs to be considered. On the other hand, no solutions for the pair (β, τ_p) achieving $\sigma < 0$ exist when $\bar{\omega} \geqslant 8.5$Hz if $g_t > 0$ due to instability. Given both stability issues and the required amplitude $|\beta|$ for the minimum $\sigma_{\min}$, the AP-DR tuned with $g_t < 0$ and a small $|\beta|$ is preferred, which agrees with [13] that a smaller tuned delay $\tau_{a,t}$ is beneficial to the conventional A-DR.

Letting $\beta = 0$ yields the A-DR, and we can obtain the associated variations of σ with respect to $\bar{\omega}$ similar to the AP-DR cases. Note that σ is a single-value function of $(g_t, \tau_{a,t})$ when $\beta = 0$. The results in the two cases $g_t < 0$ and $g_t > 0$ are superposed as the hollow circles in Fig. 3(b.3) and (c.3), respectively. Clearly, the values of σ differ as the tuned pair $(g_t, \tau_{a,t})$ varies. In addition to the evident strength $\sigma_{\min} < \sigma$ of the AP-DR for expediting transient process, the AP-DR yields a broader operable frequency band given that the tuned A-DR must satisfy the stability condition $\sigma < 0$. The settling time $\bar{t}_s$ of the transient process in the AP-DR and A-DR cases are compared in Fig. 3(b.4, b.5) and (c.4, c.5). In the frequency

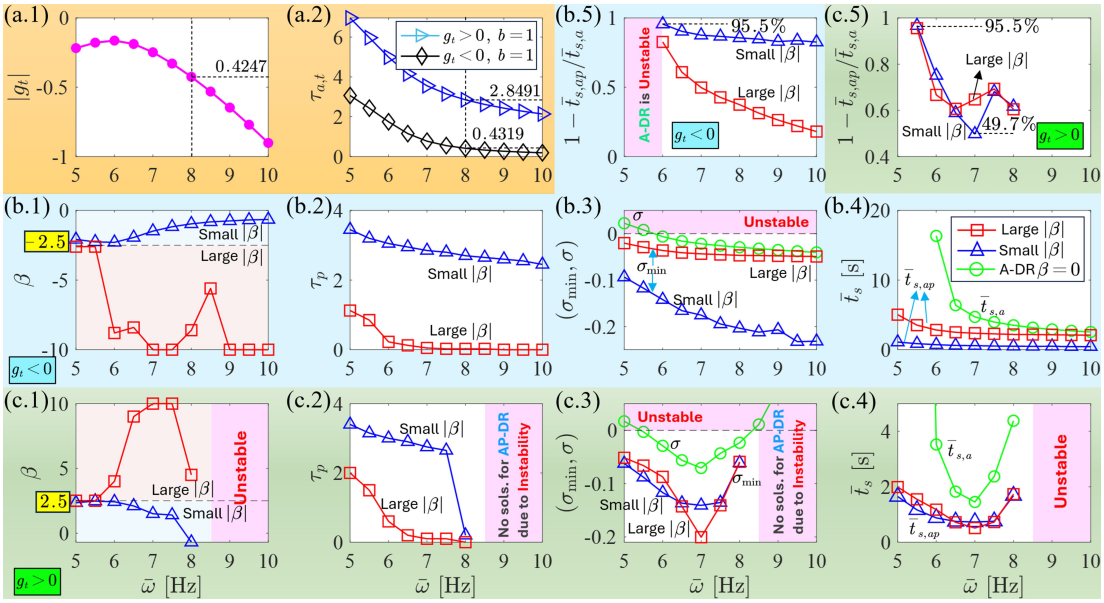

Fig. 3. ((a). Tuned pairs $(g_t, \tau_{a,t})$ versus $\bar{\omega}$. (b.1, b.2). Optimum pairs of (β, τ_p) for $\sigma_{\min}$ when $g_t < 0$. (b.3). Comparisons between $\sigma_{\min}$ of the AP-DR and σ of the A-DR. (b.4, b.5). Comparisons of the theoretical settling time $\bar{t}_s$ of the AP-DR and the A-DR. (c). Comparisons generalizing from subplots (b.1-b.5) between the A-DR and AP-DR in the case $g_t > 0$.

bands where both tuned A-DR and AP-DR are operable, the AP-DR reduces the settling time of the A-DR by 95% at most and 49.7% at least. Besides, the performance is better improved when $|\beta|$ is relatively small and $g_t < 0$.

IV. Extend Operable Low-Frequency Band

In light of Fig. 3(b.3, c.3), we further investigate the benefits of the AP-DR in extending the operable low-frequency bands for complete vibration suppression. The limited operability due to stability issues is a known crux for conventional DRs [16].

A. Sweeping procedure for stability boundaries

Stability boundaries are defined as the exhaustive control parameters rendering the characteristic Eq. (14) at least one pair of imaginary roots, given that linear systems lose stability at the critical moments when the dominant roots cross the imaginary axis. Substituting $s = j\omega_c$ into Eq. (14) yields

$$\begin{aligned} &CE\left(\omega_c, g_c, \tau_{a,c}, \beta, \tau_p\right) = \alpha_3\left(j\omega_c\right) + \\ &g_c\left(\alpha_1\left(j\omega_c\right) e^{-j\tau_{a,c}\omega_c} + \alpha_2\left(j\omega_c\right)\beta e^{-j\tau_p\omega_c}\right) = 0, \end{aligned} \tag{17}$$

where $\omega_c \in \mathbb{R}^+ \cup 0$, and the subscript $(\cdot)_c$ denotes 'critical'. To investigate the benefits of the AP-DR, we take (β, τ_p) known and evaluate their effects on the $(g_c, \tau_{a,c})$ pairs satisfying (17). However, directly solving $(g_c, \tau_{a,c})$ is involved due to the implicit relationship between g_c and $\tau_{a,c}$. To this end, we adopt a sweeping procedure for simplification, which starts with the Rekasius substitution [30] for complex exponent,

$$e^{-j\tau_{a,c}\omega_c} = \frac{1 - jT\omega_c}{1 + jT\omega_c}, T \in \mathbb{R}, \tag{18}$$

in which the mapping conditions between $\tau_{a,c}$ and T are

$$\begin{aligned} &T = \frac{1}{\omega_c}\tan\left(\frac{\tau_{a,c}\omega_c}{2}\right) \Leftrightarrow \\ &\tau_{a,c,q} = \frac{2}{\omega_c}\mathrm{a}\tan\left(\omega_c T \pm q\pi\right), q \in 0 \cup \mathbb{Z}^+. \end{aligned} \tag{19}$$

From (19), one $\tau_{a,c}$ for a ω_c corresponds to one T, while the inverse is infinite due to the branch number q similar to the tuned delay $\tau_{a,t,b}$ in (11). Substituting (18) into (17) yields

$$\begin{aligned} &CE\left(\omega_c, g_c, T\right) = \alpha_3\left(j\omega_c\right) + \\ &g_c\left[\alpha_1\left(j\omega_c\right)\frac{1 - jT\omega_c}{1 + jT\omega_c} + \alpha_2\left(j\omega_c\right)\beta\left(C_p - jS_p\right)\right] = 0, \end{aligned} \tag{20}$$

where $C_p = \cos\left(\tau_p\omega_c\right)$ and $S_p = \sin\left(\tau_p\omega_c\right)$. By adopting the Rekasius substitution (18), Eq. (17) as a transcendent complex equation is reduced to a polynomial one as (20). Separating the real and imaginary parts of the numerator of (20), we have

$$\begin{cases} E_R\left(\omega_c, g_c, T\right) = \mathrm{Re}\left(\mathrm{numer}\left(CE\left(\omega_c, g_c, T\right)\right)\right) \\ \quad = \gamma_{\mathrm{Re},1}\left(\omega_c, g_c\right)T + \gamma_{\mathrm{Re},0}\left(\omega_c, g_c\right) = 0, \\ E_I\left(\omega_c, g_c, T\right) = \mathrm{Im}\left(\mathrm{numer}\left(CE\left(\omega_c, g_c, T\right)\right)\right) \\ \quad = \gamma_{\mathrm{Im},1}\left(\omega_c, g_c\right)T + \gamma_{\mathrm{Im},0}\left(\omega_c, g_c\right) = 0, \end{cases} \tag{21}$$

which are two linear real polynomial equations in T, with $(\gamma_{\mathrm{Re},i}, \gamma_{\mathrm{Im},i})$, $i = 1, 2$, denoting real coefficients in (ω_c, g_c). Substituting the single solution of $E_R\left(\omega_c, g_c, T\right) = 0$ into $E_I\left(\omega_c, g_c, T\right) = 0$ yields a quadratic equation in g_c,

$$E_{R\to I}\left(\omega_c, g_c\right) = \sum_{i=0}^{2}\varphi_i\left(\omega_c\right)g_c^i = 0, \tag{22}$$

where φ_i denote real coefficients in ω_c. By sweeping ω_c, the exhaustive solution pairs of (ω_c, g_c) can be obtained. Back substituting such solutions into either of the two equations in (21) leads to a univariate polynomial equation in T, so the corresponding solutions of T can be exhaustively determined. Finally, the critical delays $\tau_{a,c}$ can be found as per (19), thus yielding the stability boundaries $(g_c, \tau_{a,c})$ and completing the so-called sweeping procedure.

B. Stability map and operable tuned pairs

We consider four cases $\beta = [0, 2.5, -2.5, -10]$ with $\tau_p = 0$ for demonstration, leading to the stability boundaries $(g_c, \tau_{a,c})$ shown as the thick solid curves in Fig. 4.

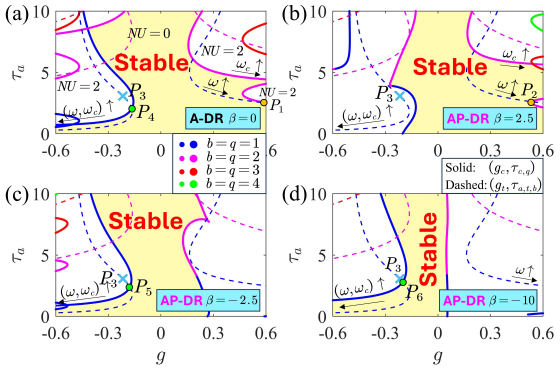

Fig. 4. Stability maps with $\tau_p = 0$. Colored regions are stable. Thick solid curves denote stability boundaries $(g_c, \tau_{a,c})$, and thin dashed ones are tuned pairs $(g_t, \tau_{a,t})$. (a). $\beta = 0$. (b). $\beta = 2.5$. (c). $\beta = -2.5$. (d). $\beta = -10$.

Let us first focus on Fig. 4(a) for the A-DR case with $\beta = 0$. Since stability losses must correspond to crossings on stability boundaries, the colored region is stable given that $g = 0$ corresponds to a passive absorber. Once we cross the stability boundaries by varying (g, τ_a), the shifting direction of the associated critical roots $\pm j\omega_c$ can be examined by

$$RT(\omega_c, g_c, \tau_{a,c}) = \mathrm{Re}\left(\frac{ds}{d\lambda}\middle|\begin{array}{c} s = j\omega_c \\ \lambda = \lambda_c \end{array}\right), \tag{23}$$

which is known as the root tendency [31], where $\lambda \in [g, \tau_a]$ denotes the crossing variable. Hence, the stability of each parametric pocket divided by stability boundaries can be determined by counting the number of unstable characteristic roots (NU), as marked in Fig. 4(a). Following the same procedure, the stable regions in the four considered cases are colored.

The tuned pairs $(g_t, \tau_{a,t})$ are superposed as the thin dashed curves in Fig. 4, and the operable ones must lie within the stable regions. Since $(g_t, \tau_{a,t})$ are functions of the excitation frequency ω as per (11), system stability limits the operable frequency band for complete vibration suppression. Comparing Fig. 4(a) and Fig. 4(b, c, d), the AP-DR by tuning $\beta \neq 0$ can manipulate the stability boundaries and thus the operable frequency band. Moreover, $\beta > 0$ and $\beta < 0$ aggravate the stability issues when $g < 0$ and $g > 0$, respectively, agreeing with Fig. 2 and Fig. 3. Note that the operable frequency band is always upper-bounded when $(g > 0, b = 1)$, exemplified by the two intersection points P_1 and P_2, while no upper bound exists when $(g < 0, b = 1)$ regardless of β, agreeing with Fig. 3(b.3, c.3). However, lower bounds always exist in both the A-DR and AP-DR cases, as to be extended next.

C. Extended operable low-frequency band by tuning β

We only focus on the preferred case $(g < 0, \beta < 0, b = 1)$, which is of no upper bound, to evaluate the benefits of the AP-DR on extending the operable low-frequency band. Accordingly, the tuned pair at $\bar{\omega} = 5$Hz ($\omega = 0.806$), i.e., $(g_t, \tau_{a,t}) = (-0.217, 3.065)$, is marked as the cross P_3 in Fig. 4 for reference. From Fig. 4(a, c, d), increasing the amplitude $|\beta|$ helps extend the operable low-frequency band, as signified by the variations of the intersection points P_4, P_5, and P_6. Given that such intersection points correspond to the same (g, τ_a) pair on tuned curves and stability boundaries [12], i.e.,

$$\begin{cases} g_t(\omega) - g_c(\omega_c) = 0, \\ \tau_{a,t}(\omega) - \tau_{a,c}(\omega_c) = 0, \end{cases} \tag{24}$$

where $\omega \neq \omega_c$, we can numerically determine the lower bound by solving ω from (24). However, directly solving (24) is infeasible since the analytical forms of $(g_c, \tau_{a,c})$ are unknown. To this end, we substitute $g_c = g_t$ into (22) and then plug the single solution $T(\omega_c, g_c = g_t)$ of either of the two equations in (21) into (19), yielding

$$\begin{cases} E_{R\to I}(\omega, \omega_c) = \sum_{i=0}^{2} \varphi_i(\omega_c)\, g_t^i(\omega) = 0, \\ E_\tau(\omega, \omega_c) = \tau_{a,t}(\omega) - \tau_{a,c}(\omega_c, T(\omega_c, g_t(\omega))) = 0, \end{cases} \tag{25}$$

which are two binary equations in (ω, ω_c), so the lower bound can be determined. The variations of the lower bound, denoted as $\bar{\omega}_{low}$ in Hz, with respect to β, are shown in Fig. 5, where markers (P_4, P_5, P_6) stem from the namesake ones in Fig. 4.

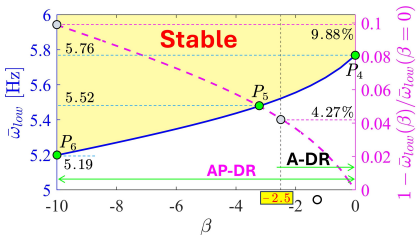

Fig. 5. Left y-axis: Variations of the lower operable frequency bound $\bar{\omega}_{low}$ when $(g < 0, \beta < 0, b = 1, \tau_p = 0)$. Right y-axis: Extension ratio for $\bar{\omega}_{low}$ by adopting the AP-DR with $\beta \neq 0$ compared with the A-DR with $\beta = 0$.

From Fig. 5, the lower operable frequency bound is reduced from $\bar{\omega}_{low} = 5.76$Hz to $\bar{\omega}_{low} = 5.19$Hz as β varies from $\beta = 0$ to $\beta = -10$, resulting in 9.88% extension of the operable low-frequency band by adopting the AP-DR. Note that such extension counter-intuitively corresponds to narrowed operable regions of (g, τ_a), see Fig. 4(a, c, d). On the other hand, one can find the marginal effects of such extension by increasing $|\beta|$ given that $\beta = -2.5$ achieves 4.27% extension compared with $\beta = 0$, i.e., 25% of the amplitude $|\beta| = 10$ achieves 43% of the effects. Consequently, further extending the operable low-frequency band by increasing $|\beta|$ is not recommended, additionally given that a smaller $|\beta|$ is preferred to expedite the transient process when $\bar{\omega}$ is small, see Fig. 3(b.1, b.3). Note that $\tau_p = 0$ holds in Fig. 4 and Fig. 5.

D. Further extension by additionally tuning τ_p

To seek possible further extension of the operable low-frequency band, we revisit Fig. 3(b.1, b.3), where the system is stable at $\bar{\omega} = 5$Hz, with keeping $|\beta|$ low around $|\beta| = 2.5$. In contrast, from Fig. 4 and Fig. 5, by only manipulating $|\beta| \leqslant 10$, complete vibration suppression at $\bar{\omega} = 5$Hz is inoperable due to instability. The difference between such two cases is that the time delay τ_p is introduced in the former

case. Given the aforementioned benefits of a smaller $|\beta|$ and that $\beta \approx -2.5$ is beneficial for expediting transient process in the low-frequency band when $g_t < 0$, we evaluate the effects of τ_p on extending the operable low-frequency band while fixing $\beta = -2.5$. Variations of the stability map to τ_p are shown in Fig. 6, where the markers P_3 and P_4 correspond to the namesake ones in Fig. 4 and Fig. 5 for reference.

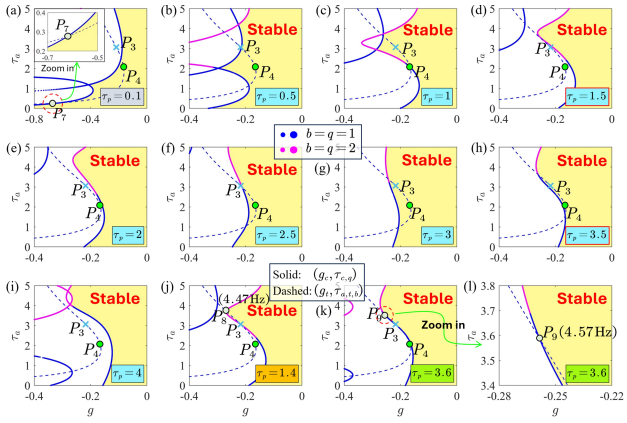

Fig. 6. Variations of the stability map respect to τ_p for $\beta = -2.5$ and $g < 0$. Colored regions are stable. (a). $\tau_p = 0.1$. (b-i). τ_p varies from $\tau_p = 0.5$ to $\tau_p = 4$ at the step of $\tau_p = 0.5$. (j). $\tau_p = 1.4$. (k). $\tau_p = 3.6$. (l) is the zoomed plot of (k). Thick solid curves denote stability boundaries $(g_c, \tau_{a,c})$, and thin dashed ones are tuned pairs $(g_t, \tau_{a,t})$.

Fig. 6(a) evaluates the effects of the inherent loop delay exemplified by $\bar{\tau}_p = 0.1/\bar{\omega}_p = 2.6\text{ms}$ on the operable frequency band. The introduction of τ_p results in an upper bound P_7 compared with the A-DR. The related frequency can be determined as per (25), yielding $\bar{\omega}_{up}(P_7) = 8.89\text{Hz}$. Multiple solutions are available to address this issue. i). Simply set $\beta = 0$ so that the AP-DR reduces to the A-DR. ii). Alter (β, τ_p) following Fig. 3(b). For the problem here to extend the operable low-frequency band, benefits of $\tau_p > 0$ are sought.

Let us further increase τ_p from $\tau_p = 0.5$ to $\tau_p = 4$ at the step of $\tau_p = 0.5$, leading to Fig. 6(b-i). Compared with Fig. 4 and Fig. 5, by additionally manipulating τ_p with multiple τ_p values optional, P_3 corresponding to $\bar{\omega} = 5\text{Hz}$ is possible to lie within stable regions making the complete vibration suppression at this frequency operable. From Fig. 6(b-d) and (f-h), we can conclude that the operable low-frequency bound can be extended to be less than $\bar{\omega} = 5\text{Hz}$ and that the critical values of τ_p for the minimum lower bound appear around $\tau_p = 1.5$ and $\tau_p = 3.5$. The more specific cases are shown in Fig. 6(j-l). With Eq. (25) and the intersection points (P_8, P_9), the lower bound can be as low as $\bar{\omega}_{low}(P_8) = 4.47\text{Hz}$ and $\bar{\omega}_{low}(P_9) = 4.57\text{Hz}$ when $\tau_p = 1.4$ and $\tau_p = 3.6$, respectively. Compared with the A-DR, i.e., $\bar{\omega}_{low}(P_4) = 5.76\text{Hz}$ as per Fig. 5, the operable low-frequency band is extended by over 20%. However, we remark that when practically handling low-frequency vibrations, the tuned pair $(g_t, \tau_{a,t})$ should be separated from the stability boundaries for an appropriate distance given the possible fluctuations of the control parameters in practice [16]. The above observations signify another benefit of the AP-DR by properly tuning (β, τ_p) to extend operable low-frequency band in addition to expediting the transient process. Besides, combining with Fig. 6 and Fig. 3(b.1, b.3), such two benefits can be achieved simultaneously by having $\tau_p \in [3, 3.6]$, yielding an extended operable low-frequency band and expedited transient processes there for complete vibration suppression over the A-DR.

V. Robust Complete Vibration Suppression

In addition to the previously shown benefits of the AP-DR for expediting the transient process and extending operable low-frequency band, we next reveal that the AP-DR can enhance the robustness of the 'complete' vibration suppression in practice. The transfer function from f_e to x_p is

$$\begin{aligned} G_{fe,xp}(s, g, \tau_a, \beta, \tau_p) &= \frac{X_p}{F} \\ &= \mathbf{Z}^{-1}_{(2,2)} = \frac{\mu\left(s^2 + 2\left(\zeta_a + \zeta_g\right) v s + v^2\right) - g e^{-\tau_a s}}{C E(s, g, \tau_a, \beta, \tau_p)}, \end{aligned} \tag{26}$$

where the subscript $(2,2)$ denotes the $(2,2)$ element of the matrix $\mathbf{Z}^{-1}$. Note that the numerator of (26) is a scaled characteristic equation of the system dynamics in Fig. 1(b), the solution of which for (g, τ_a) corresponds to the tuned pair in (11). The analysis is twofold by considering vibration frequency detection errors and the inevitable vibration noises.

A. Against frequency mismatch

We first test the AP-DR performance in handling the common mismatches between the detected excitation frequency and the actual one, which can be caused by poor sensor performance or signal processing errors. Such mismatches reduce the accuracy of the tuned pair $(g_t, \tau_{a,t})$, thus leading to residual vibrations. The analysis is still based on the system (16), and the frequency responses of the primary structure as per (26) for various control parameters are shown in Fig. 7.

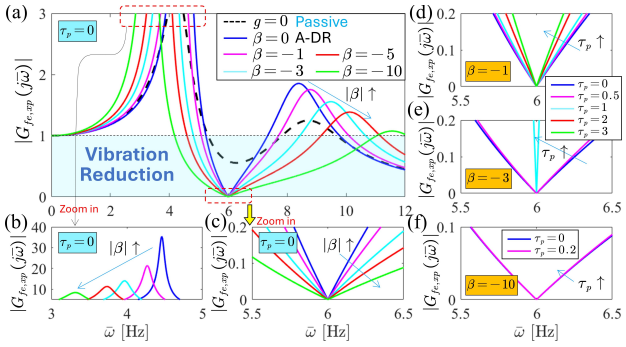

Fig. 7. (a). Frequency responses for different parameters when $\tau_p = 0$. (b, c). The zoomed plots of (a). (c-d). Evaluation of the effects of τ_p on the response sensitivity to frequency mismatch. Only stable cases are shown.

The black dashed curve in Fig. 7(a) signifies the frequency responses in the passive case $g = 0$. An antiresonance peak appears around $\bar{\omega} = 6\text{Hz}$, which agrees with the undamped natural frequency of the absorber, i.e., $\bar{\omega}_a = 6.11\text{Hz}$. To enhance vibration reduction at $\bar{\omega} = 6\text{Hz}$, we first activate feedback forces with $(g_t, \tau_{a,t,1}) = (-0.1633, 1.7455)$ and $\tau_p = 0$. The desired complete vibration suppression is signified by $|G_{fe,xp}| = 0$ regardless of β as expected. However, such

complete vibration suppression by the A-DR with $\beta = 0$ raises the resonance peaks of the passive absorber, making $|G_{fe,xp}|$ rapidly increase even if $\bar{\omega}$ slightly deviates from $\bar{\omega} = 6$Hz, thus possibly resulting in significant residual vibrations, see also the zoomed plot in Fig. 7(c). In contrast, adopting the AP-DR by increasing the amplitude $|\beta|$ reduces $|G_{fe,xp}|$ around the tuning frequency, thus favorably lowering the response sensitivity of the primary structure to frequency mismatch.

The effects of $\tau_p > 0$ are evaluated in Fig. 7(d-f), where only the τ_p values rendering a stable system are shown. One can find that increasing τ_p always increases $|G_{fe,xp}|$, which is unfavorable to suppressing residual vibrations. The reason is that the AP-DR with $\tau_p > 0$ cannot timely respond once frequency mismatches occur. Notably, the conclusion here that a smaller delay τ_p is preferred differs from previous ones to expedite convergence and to extend the operable frequency band limited by stability since the frequency response amplitude $|G_{fe,xp}|$ here corresponds to steady states while previous issues happen in the transient process. To this end, we can increase $|\beta|$ and reduce τ_p after the transient process to fully exploit the AP-DR strength. Particularly, we achieved similar effects of lowering $|G_{fe,xp}|$ in [18] by altering the absorber substructure. As an alternative, the AP-DR here offers a much simpler solution that can be implemented with minor modifications to the control law, see also [14], [15].

B. Against vibration noises

From Fig. 7(a), the tuned AP-DR yields complete vibration suppression while achieving broadband vibration reduction at the tuning frequency $\bar{\omega} = 6$Hz compared with the passive absorber and the A-DR. Next, the frequency interval of the antiresonance valley satisfying $|G_{fe,xp}| < 1$ is taken as the index to depict the vibration reduction capacity. Accordingly, the associated results in Fig. 7(a) are extracted in Fig. 8.

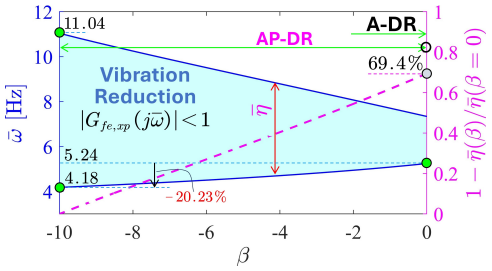

Fig. 8. Left y-axis: Variations of the frequency interval of the antiresonance valley with $|G_{fe,xp}| < 1$ for the results in Fig. 7(a). Right y-axis: Width ratios of antiresonance interval where $|G_{fe,xp}| < 1$ of the AP-DR to that of the A-DR ($\beta = 0$).

From Fig. 8, the extension of the antiresonance valley by the AP-DR reaches up to 69.4% by having $\beta = -10$, making the AP-DR act as a broadband notch filter to better suppress vibration noises close to the tuning frequency. This can be very helpful since the main noise components should be distributed around the excitation frequency. Meantime, the lower frequency bound for vibration reduction $|G_{fe,xp}| < 1$ is extended by 20.23%. Combining also with the significantly reduced resonance peak heights shown in Fig. 7(a, b), one can infer that the AP-DR is more robust against vibration noises than the conventional A-DR in steady states when the vibration frequency $\bar{\omega}$ is exactly known for both DRs.

Remark 1. *We have now observed significant theoretical benefits of the AP-DR over A-DR in three aspects, i.e., expedited transient process, extended operable low-frequency band, and enhanced robustness against residual vibrations. Possible concerns can be that the AP-DR requires an additional sensor to monitor the primary. However, in most cases needing active vibration control, the states of the primary structure are online monitored to determine whether to activate active control.*

VI. Verifications

Next, experiments and simulations are conducted to verify the threefold benefits of the AP-DR claimed in Remark 1. SIMULINK-based simulation models and video recordings of experiments are available at https://bit.ly/3yAUVse.

A. Experimental setup

The main body of the experimental setup related to Fig. 1(a) is detailed in Fig. 9(a, b). Two voice coil motors (VCMs) are used to generate the excitation $\bar{f}_e$ and the feedback actuation $\bar{u}$, and two laser sensors are fixed on the frame to monitor the absolute displacements of the primary structure and the absorber. The logics for generating $\bar{f}_e$ and $\bar{u}$ are the same. For demonstration, we focus on Fig. 9(c) for the hardware loop of driving VCM2 to generate $\bar{u}$. The dSPACE MicroLabBox as controller online processes system states $(\bar{x}_p, \bar{x}_a)$ and generates control signals to VCM driver, which outputs current dictated by control signals to the VCM mover, finally yielding actuation forces based on the electromagnetic effects between the stator (magnets) and mover (coils).

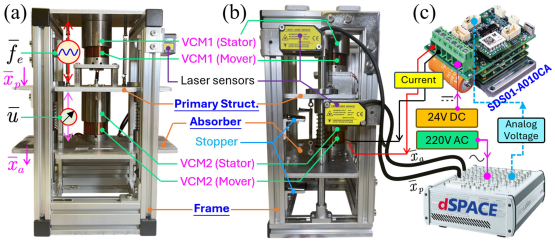

Fig. 9. Experimental setup. Front (a) and right (b) views of the main body. (c). Hardware loop for feedback control of $\bar{u}$.

The mechanical parameters are obtained as $(\bar{m}_a, \bar{m}_p) = (0.51, 0.965)\,\text{kg}$, $(\bar{c}_a, \bar{c}_g, \bar{c}_p) = (4.3, 2.0, 5.0)\,\text{Ns/m}$, $(\bar{k}_a, \bar{k}_p) = (753, 1463)\,\text{N/m}$, which correspond to (16). In all tests, the sampling time of the controller and the two laser sensors are set as 1kHz, the excitation $\bar{f}_e$ is of the amplitude $|\bar{f}_e| = 4$N, and the pair $(\bar{g}, \bar{\tau}_a)$ is tuned with $(\bar{g} < 0, b = 1)$.

B. Expedited transient process

We start with verifying the expedited transient process of the AP-DR by considering the case $\bar{\omega} = 6$Hz, leading to $(\bar{g}_t, \bar{\tau}_{a,t}) = (-239.17\text{N/m}, 44.8\text{ms})$. As per Fig. 3(b), the settling time $\bar{t}_{s,a}$ in the A-DR case ($\beta = 0$) can be reduced by 95% in theory by having $(\beta, \bar{\tau}_p) = (-2.29, 78.3\text{ms})$.

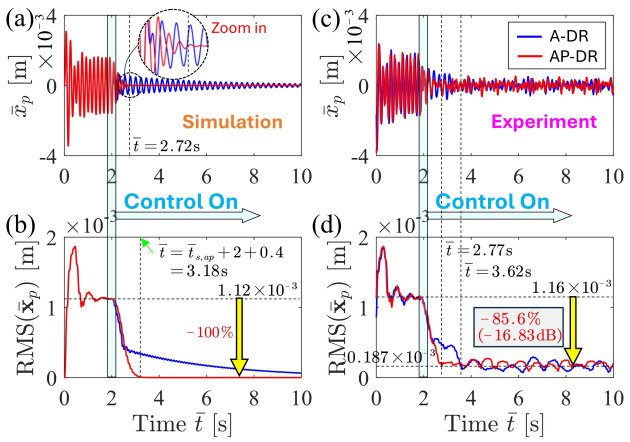

Fig. 10. Verifications of the expedited transient process of the AP-DR with simulations (a, b) and experiments (c, d). (a, c). Time history of $\bar{x}_p$. (b, d). Root mean square (RMS) of the dataset $\bar{\mathbf{x}}_p$ sampled at the last 400 time steps.

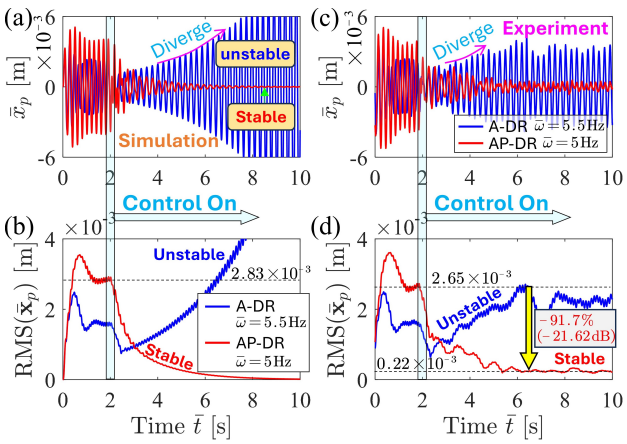

Fig. 11. Verifications of the extended operable low-frequency band of the AP-DR with simulations (a, b) and experiments (c, d). (a, c). Time history of $\bar{x}_p$. (b, d). RMS of the dataset $\bar{\mathbf{x}}_p$.

Fig. 10(a, b) show the simulation results of the responses $\bar{x}_p$ and the root mean square of the associated dataset $\bar{\mathbf{x}}_p$ sampled during the 400 time steps (i.e., 0.4s, the same in the following) before the current one $\bar{t}$ in both the A-DR and AP-DR cases. From Fig. 10(b), the settling time in the AP-DR case is approximately $\bar{t}_{s,ap} = 3.18 - 0.4 - 2 = 0.78$s, agreeing with the theoretical prediction $\bar{t}_{s,ap} = 0.72$s in Fig. 3(b.4), see also Fig. 10(a). In contrast, we have $\bar{t}_{s,a} > 10$s in the A-DR case, again verifying theoretical results. The corresponding experimental results are shown in Fig. 10(c, d). From Fig. 10(d), vibrations are reduced by 85.6% after activating the feedback actuation, and residual vibrations are related to system noises and errors (e.g., the identification inaccuracy in system parameters and thus in implementing control parameters, as to be handled). To this end, the time instants when $\mathrm{RMS}\,(\bar{\mathbf{x}}_p)$ first reaches steady-state values are used to estimate the duration of the transient process, leading to $1-(2.77-2.4)\,/\,(3.62-2.4) = 69.7\%$ reduction of the settling time of the A-DR by adopting the AP-DR.

C. Extended operable low-frequency band

Next, we verify the extended operable low-frequency band by the AP-DR. From Fig. 5, the A-DR cannot handle vibrations at a frequency lower than $\bar{\omega} = 5.76$Hz. Hence, the excitation at $\bar{\omega} = 5.5$Hz is considered for tests, leading to the tuned pair $(\bar{g}_t, \bar{\tau}_{a,t}) = (-260.99\mathrm{N/m}, 62.4\mathrm{ms})$. The simulation and experimental results are shown in Fig. 11.

System instability in the A-DR case is verified by the divergent responses denoted as the blue solid curves in Fig. 11(a, b), which can result in possible structural failures in practice. However, in the experimental results shown in Fig. 11(c, d), the amplitudes of such divergence are upper-bounded since the divergent system responses critically exceed effective VCM strokes. To achieve complete vibration suppression in the low-frequency band, we adopt the AP-DR. Revisit Fig. 6(c), the AP-DR with $(\beta, \bar{\tau}_p) = (-2.5, 25.7\mathrm{ms})$ can even handle the vibration at a lower frequency $\bar{\omega} = 5$Hz. In this case, the tuned pair is $(\bar{g}_t, \bar{\tau}_{a,t}) = (-318.58\mathrm{N/m}, 78.7\mathrm{ms})$, leading to the responses $\bar{x}_p$ shown as the red solid curves in Fig. 11. From Fig. 11(a, b), the desired complete vibration suppression is achieved, and the vibrations are suppressed by 91.7% in experiments, see Fig. 11(c, d). Compared with the theoretical lower bound $\bar{\omega} = 5.76$Hz of the A-DR as per Fig. 7, the extension by the AP-DR is $1-5/5.76 = 13.2\%$ at least. Note that the steady-state residual vibrations stemming from the aforementioned system noises and errors are roughly the same level as that in the previous case $\bar{\omega} = 6$Hz shown in Fig. 10, as to be handled next.

D. Enhanced robustness for complete vibration suppression

The benefits of the AP-DR in handling frequency mismatch and vibration noises are tested. We first consider the former issue. Following Fig. 7, the excitation is now at $\bar{\omega} = 6.2$Hz, while the tuned pair $(\bar{g}_t, \bar{\tau}_{a,t})$ at $\bar{\omega} = 6$Hz is still adopted, assuming that errors in signal detection and processing result in 3.2% frequency mismatch. Accordingly, the responses in the A-DR case with $\beta = 0$ are shown in Fig. 12(a, b), where experimental results agree well with simulations.

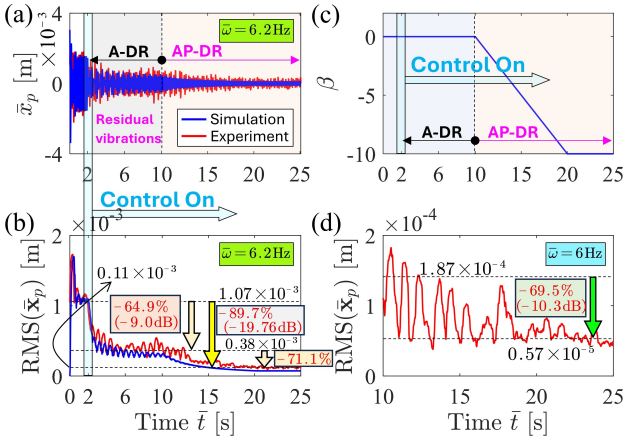

Fig. 12. Verifications of the stronger robustness of the AP-DR against residual vibrations with simulations (a, b) and experiments (c, d). $(\bar{g}, \bar{\tau}_a)$ are tuned at $\bar{\omega} = 6$Hz, and colored boxes in (a, b, d) signify the excitation frequency. (a). Time history of $\bar{x}_p$. (c). Time history of β. (b, d). RMS of the dataset $\bar{\mathbf{x}}_p$.

Focusing on experimental results, one can find from the time interval $\bar{t} \in [2\text{s}, 10\text{s}]$ of Fig. 12(a, b) that the resulting residual vibrations are significant, making the vibration reduction far from the desired complete manner, even if the tested frequency mismatch is small. When $\bar{t} \in [10\text{s}, 15\text{s}]$, the AP-DR is adopted with $\bar{\tau}_p = 0$ while varying β from 0 to -10 following Fig. 12(c). From Fig. 12(a, b), residual vibrations are suppressed by 71.1% as $|\beta|$ increases, resulting in 89.7% vibration reduction in steady states compared with the passive case $\bar{t} < 2\text{s}$. Note that such vibration suppression even outperforms the case where the excitation frequency is exactly known, see Fig. 10(d), where $\text{RMS}\,(\bar{\mathbf{x}}_p) = 0.187\text{mm}$ in steady states. For further demonstration, we eliminate such frequency mismatch by having the excitation frequency as $\bar{\omega} = 6\text{Hz}$, leading to Fig. 12(d), in which the omitted transient process $\bar{t} < 10\text{s}$ can be referred to Fig. 10(d), and β still varies following Fig. 12(c). By increasing $|\beta|$, residual vibrations are reduced by 69.5%, agreeing with Fig. 8. Compared with the passive case where $\text{RMS}\,(\bar{\mathbf{x}}_p) = 1.16\text{mm}$ as per Fig. 10(d), the final vibration suppression by the AP-DR is up to 95.1%. Such a percentage number is high since the test frequency $\bar{\omega} = 6\text{Hz}$ is around the natural frequency of the absorber, i.e., $\bar{\omega}_a = 6.11\text{Hz}$.

E. Comparisons with other control laws

To reduce measurement noises, we recently considered a multiple-delayed distributed DR (MD-DDR) [12], with

$$\bar{u}_{MD}\,(\bar{t}) = \bar{g}_D \int_{\bar{\tau}_2}^{\bar{\tau}_1} \bar{x}_a\,(\bar{t} - \bar{\vartheta})\, d\bar{\vartheta}, \tag{27}$$

where $\bar{\tau}_1 > \bar{\tau}_2 > 0$.In this case, all absorber states $\bar{x}_a$ within the past time interval $\bar{t} \in [\bar{t} - \bar{\tau}_1, \bar{t} - \bar{\tau}_2]$ are summed to generate feedback force, so $\bar{u}_{MD}$ acts like a moving averaging filter [10]. To achieve complete vibration suppression, we now have three tunable parameters $(\bar{g}_D, \bar{\tau}_1, \bar{\tau}_2)$, in which $(\bar{g}_D, \bar{\tau}_1)$ are determined once $(\bar{\tau}_2, \bar{\omega})$ are given. The calculation details are left to [12], and the tuned pairs $(\bar{g}_{D,t}, \bar{\tau}_{1,t})$ for $\bar{\omega} = 6\text{Hz}$ as $\bar{\tau}_2$ varies are derived in Fig. 13(a). Accordingly, Fig. 13(b) shows the real part σ of the dominant roots following Fig. 3.

From Fig. 13(a, b), the MD-DDR with $\bar{\tau}_2 = 89.8\text{ms}$ is preferred as it corresponds to a broader interval $[\bar{t} - \bar{\tau}_1, \bar{t} - \bar{\tau}_2]$ for noise suppression and a smaller $\sigma < 0$ for expediting transient process. Accordingly, responses $\bar{x}_p$ of the primary are shown in Fig. 13(c, d), where the simulation depicts the desired complete vibration suppression. For experimental results, compared with Fig. 10(c, d), MD-DDR indeed improves the A-DR performance in steady states, while it performs much worse than the AP-DR in Fig. 12(d). Furthermore, the AP-DR can also expedite the response speed of the MD-DDR, see Fig. 13(d) and Fig. 10(d) for the marked time instances when arriving at steady states. Thus, the AP-DR with a simple control logic can even be competitive to complex DR designs.

F. Enhanced performance in the frequency-varying cases

All claimed benefits of the AP-DR have now been verified in the fixed-frequency case. In real applications, the excitation can undergo acceleration and deceleration, resulting in frequency-varying vibrations. To test the AP-DR performance

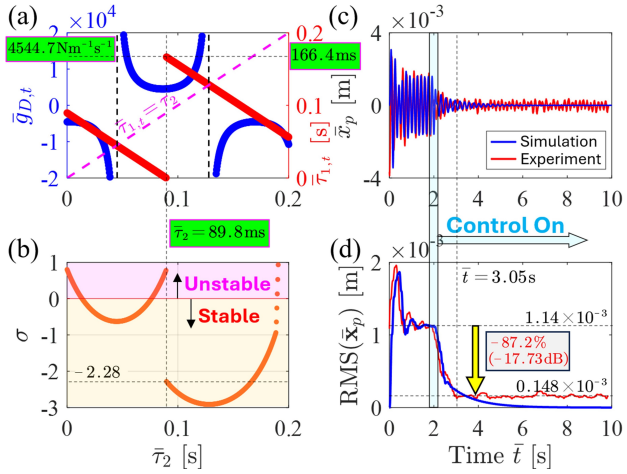

Fig. 13. (a). Tuned pairs $(\bar{g}_{D,t}, \bar{\tau}_{1,t})$ of the MD-DDR with (27) versus $\bar{\tau}_2$ for $\bar{\omega} = 6\text{Hz}$. (b). Variations of the real part of the dominant roots of the characteristic equation corresponding to the MD-DDR. (c, d). Time history of $\bar{x}_p$ in the MD-DDR case.

in such cases, we consider an acceleration process by linearly increasing $\bar{\omega}$ at the rate of 0.15Hz/s within $\bar{t} \in [2\text{s}, 12\text{s}]$, yielding the blue solid curve in Fig. 14(a). As per [19], the tuning frequency should be overclocked in this process, resulting in the red dashed tuning curve in Fig. 14(a). Variations of the tuned pairs $(g_t, \tau_{a,t})$ can be referred to Fig. 3(a).

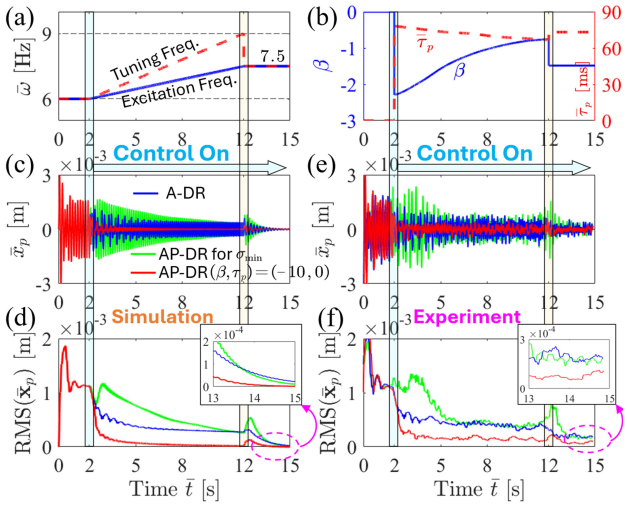

Fig. 14. Tests of the enhanced AP-DR performance in the frequency-varying case. (a). Variations of excitation frequency and the tuning frequency. (b). Variations of (β, τ_p) for $\sigma_{\min}$ as per subplot (a) and Fig. 3(b). (c, d). Simulation response $\bar{x}_p$ in three DR cases. (e, f). Experimental results.

First, one may use the AP-DR to expedite the transient process by real-time updating (β, τ_p) following Fig. 3 to achieve $\sigma_{\min}$. The associated variations of (β, τ_p) for $|\beta| < 2.5$ are reviewed in Fig. 14(b). Simulation comparisons between such an AP-DR and the A-DR are performed in Fig. 14(c, d), where the AP-DR unfavorably yields larger vibrations in the acceleration process, although the final convergence at $\bar{\omega} = 7.5\text{Hz}$ is expedited as expected, see the zoomed plot in Fig. 14(d). That is, expedited convergence is not achieved in the acceleration process. The reason is that the delay makes

current feedback forces correspond to a 'stale' frequency, thus resulting in asynchronousness. Note that similar observations can also be found in [19]. We then need to reduce the delay in frequency-varying cases. For $\tau_{a,t}$, one can minimize the branch number b, which has been done in the test. When adopting the AP-DR, we let $\tau_p = 0$. Additionally given the extended antiresonance valley by increasing $|\beta|$ as per Fig. 8, which helps suppress adjacent frequency components when $\bar{\omega}$ varies, we let $\beta = -10$, leading to the responses of the primary shown as the red solid curves in Fig. 14(c, d). In this case, the AP-DR yields sufficiently low residual vibrations. Experimental results are shown in Fig. 14(e, f), where the AP-DR with $(\beta, \tau_p) = (-10, 0)$ performs the best as expected.

VII. Conclusions

We actuate the DR with a hybrid multiple-delayed control law by additionally introducing delayed states of the primary structure to enhance complete vibration suppression. This hybrid control law yielding the AP-DR concept endows two new control parameters $(\beta, \bar{\tau}_p)$ for feedback tuning, which significantly improves system performance without affecting the tunning mechanism and the structure of the conventional DR (i.e., A-DR), resulting in the so-called complete compliance.

Spectral analysis shows that the settling time in the A-DR case can be reduced by more than 95% and 49.7% at least. Stability analysis based on stability boundaries shows that the operable low-frequency band for complete vibration suppression can be extended by over 20%. Dynamical analysis based on frequency response functions shows that the AP-DR significantly lowers the response sensitivity of the primary structure around the tuning frequency and reduces resonance peaks for better suppressing residual vibrations. The above theoretical benefits are experimentally verified, leading to 69.7% reduction of the transient process, at least 13.2% extension of the operable low-frequency band, and 71.1% suppression of residual vibrations caused by frequency mismatch and noises, finally resulting in up to 95.1% vibration reduction compared with the passive absorber even around its natural frequency. Furthermore, better performance in suppressing residual vibrations and expediting response can even be competitive with complex control logics exemplified by (27). The AP-DR can also enhance vibration suppression in frequency-varying cases.

To expedite the transient process and extend the operable low-frequency band, a larger $\bar{\tau}_p$ combining with a smaller $|\beta|$ is preferred. Once the primary is settled, not necessarily to be complete, $\bar{\tau}_p$ should be reduced while increasing $|\beta|$ to suppress residual vibrations by extending antiresonance valley of the primary. The extended antiresonance valley also helps suppress inevitable residual vibrations in frequency-varying cases by lowering responses at adjacent frequencies.

The hybrid multiple-delayed control law significantly improves system performance with very few modifications to the conventional DR, providing an easy-to-implement solution for real applications. As a further step from Fig. 7, our next work aims to simultaneously achieve complete vibration suppression and (qualitative) minimization of the resonance peaks [32] to enhance robustness against excitation perturbations. Moreover, engineering applications [33], [34] will be considered.

References

[1] H. Frahm, "Device for damping vibrations of bodies," 1911.

[2] S. Elias and V. Matsagar, "Research developments in vibration control of structures using passive tuned mass dampers," *Annual Reviews in Control*, vol. 44, pp. 129–156, 2017.

[3] N. Olgac and B. Holm-Hansen, "A novel active vibration absorption technique: delayed resonator," *Journal of Sound and Vibration*, vol. 176, no. 1, pp. 93–104, 1994.

[4] H. Elmali, M. Renzulli, and N. Olgac, "Experimental comparison of delayed resonator and pd controlled vibration absorbers using electromagnetic actuators," *J. Dyn. Sys., Meas., Control*, vol. 122, no. 3, pp. 514–520, 2000.

[5] D. Filipovic and N. Olgac, "Torsional delayed resonator with velocity feedback," *IEEE/ASME transactions on mechatronics*, vol. 3, no. 1, pp. 67–72, 1998.

[6] N. Olgac, H. Elmali, M. Hosek, and M. Renzulli, "Active vibration control of distributed systems using delayed resonator with acceleration feedback," *J. Dyn. Sys., Meas., Control.*, 1997.

[7] J. Xu and Y. Sun, "Experimental studies on active control of a dynamic system via a time-delayed absorber," *Acta Mechanica Sinica*, vol. 31, pp. 229–247, 2015.

[8] O. Eris, B. Alikoc, and A. F. Ergenc, "A new delayed resonator design approach for extended operable frequency range," *Journal of Vibration and Acoustics*, vol. 140, no. 4, p. 041003, 2018.

[9] X. Zhang, J. Xu, and J. Ji, "Modelling and tuning for a time-delayed vibration absorber with friction," *Journal of Sound and Vibration*, vol. 424, pp. 137–157, 2018.

[10] D. Pilbauer, T. Vyhlídal, and N. Olgac, "Delayed resonator with distributed delay in acceleration feedback—design and experimental verification," *IEEE/ASME Transactions on Mechatronics*, vol. 21, no. 4, pp. 2120–2131, 2016.

[11] V. Kučera, D. Pilbauer, T. Vyhlídal, and N. Olgac, "Extended delayed resonators–design and experimental verification," *Mechatronics*, vol. 41, pp. 29–44, 2017.

[12] Y. Liu, N. Olgac, and L. Cheng, "Delayed resonator with multiple distributed delays–considering and optimizing the inherent loop delay," *Journal of Sound and Vibration*, vol. 576, p. 118290, 2024.

[13] T. Vyhlídal, D. Pilbauer, B. Alikoc, and W. Michiels, "Analysis and design aspects of delayed resonator absorber with position, velocity or acceleration feedback," *Journal of Sound and Vibration*, vol. 459, p. 114831, 2019.

[14] M. Kuře, J. Bušek, I. Boussaada, W. Michiels, S.-I. Niculescu, and T. Vyhlídal, "Robust delayed resonator with acceleration feedback—design by double root assignment and experimental validation," *Journal of Sound and Vibration*, vol. 576, p. 118261, 2024.

[15] D. Pilbauer, T. Vyhlídal, and W. Michiels, "Optimized design of robust resonator with distributed time-delay," *Journal of Sound and Vibration*, vol. 443, pp. 576–590, 2019.

[16] J. Cai, Y. Liu, Q. Gao, and Y. Chen, "Spectrum-based stability analysis for fractional-order delayed resonator with order scheduling," *Journal of Sound and Vibration*, vol. 546, p. 117440, 2023.

[17] M. Valášek, N. Olgac, and Z. Neusser, "Real-time tunable single-degree of freedom, multiple-frequency vibration absorber," *Mechanical Systems and Signal Processing*, vol. 133, p. 106244, 2019.

[18] Y. Liu, J. Cai, N. Olgac, and Q. Gao, "A robust delayed resonator construction using amplifying mechanism," *Journal of Vibration and Acoustics*, vol. 145, no. 1, p. 011010, 2023.

[19] Y. Liu and L. Cheng, "A high-static-low-dynamic-stiffness delayed resonator vibration absorber," *Communications in Nonlinear Science and Numerical Simulation*, vol. 140, p. 108299, 2025.

[20] P. Beneš, J. Gregor, W. Michiels, T. Vyhlídal, and Z. Šika, "Collocated and non-collocated active spatial absorbers for spatial flexible structures," *Mechanics Based Design of Structures and Machines*, pp. 1–29, 2024.

[21] N. Olgac and R. Jenkins, "Actively tuned noncollocated vibration absorption: An unexplored venue in vibration science and a benchmark problem," *IEEE Transactions on Control Systems Technology*, vol. 29, no. 1, pp. 294–304, 2020.

[22] A. Saldanha, W. Michiels, M. Kuře, J. Bušek, and T. Vyhlídal, "Stability optimization of time-delay systems with zero-location constraints applied to non-collocated vibration suppression," *Mechanical Systems and Signal Processing*, vol. 208, p. 110886, 2024.

[23] H. Silm, M. Kuře, J. Bušek, W. Michiels, and T. Vyhlídal, "Spectral design and experimental validation of noncollocated vibration suppression by a delayed resonator and time-delay controller," *IEEE Transactions on Control Systems Technology*, 2023.

[24] D. Huang, S. Zhou, R. Li, and D. Yurchenko, "On the analysis of the tristable vibration isolation system with delayed feedback control under parametric excitation," *Mechanical Systems and Signal Processing*, vol. 164, p. 108207, 2022.
[25] M. Karama, M. Hamdi, and M. Habbad, "Energy harvesting in a nonlinear energy sink absorber using delayed resonators," *Nonlinear Dynamics*, vol. 105, no. 1, pp. 113–129, 2021.
[26] I. Mancisidor, A. Pena-Sevillano, Z. Dombovari, R. Barcena, and J. Munoa, "Delayed feedback control for chatter suppression in turning machines," *Mechatronics*, vol. 63, p. 102276, 2019.
[27] F. Wang, X. Sun, H. Meng, and J. Xu, "Time-delayed feedback control design and its application for vibration absorption," *IEEE Transactions on Industrial Electronics*, vol. 68, no. 9, pp. 8593–8602, 2020.
[28] B. Yan, X. Wang, H. Ma, W. Lu, and Q. Li, "Hybrid time-delayed feedforward and feedback control of lever-type quasi-zero-stiffness vibration isolators," *IEEE Transactions on Industrial Electronics*, vol. 99, pp. 1–10, 2023.
[29] T. Vyhlidal and P. Zitek, "Mapping based algorithm for large-scale computation of quasi-polynomial zeros," *IEEE Transactions on Automatic Control*, vol. 54, no. 1, pp. 171–177, 2009.
[30] Z. Rekasius, "A stability test for systems with delays," in *Joint Automatic Control Conference*, 1980, Conference Proceedings, p. 39.
[31] N. Olgac and R. Sipahi, "An exact method for the stability analysis of time-delayed linear time-invariant (lti) systems," *IEEE Transactions on Automatic Control*, vol. 47, no. 5, pp. 793–797, 2002.
[32] H. Meng, X. Sun, J. Xu, and F. Wang, "The generalization of equal-peak method for delay-coupled nonlinear system," *Physica D: Nonlinear Phenomena*, vol. 403, p. 132340, 2020.
[33] A. Q. Al-Dujaili, A. J. Humaidi, Z. T. Allawi, and M. E. Sadiq, "Earthquake hazard mitigation for uncertain building systems based on adaptive synergetic control," *Applied system innovation*, vol. 6, no. 2, p. 34, 2023.
[34] A. J. Humaidi, M. E. Sadiq, A. I. Abdulkareem, I. K. Ibraheem, and A. T. Azar, "Adaptive backstepping sliding mode control design for vibration suppression of earth-quaked building supported by magneto-rheological damper," *Journal of Low Frequency Noise, Vibration and Active Control*, vol. 41, no. 2, pp. 768–783, 2022.

Yifan Liu received the B.S. degree from Nanchang University in 2020, and the M.S. degree from Harbin Institute of Technology (Shenzhen) in 2023, both in mechanical engineering.

He is now pursuing the Ph.D. degree at The Hong Kong Polytechnic University. His research interest mainly includes time-delay system, vibration control, and system optimization.

Bo Yan received the Ph.D. degree in mechanics from the Xi'an Jiaotong University, Xi'an, China, in 2014.

From 2015 to 2016, he served as an Assistant Researcher with the Chinese Academy of Sciences, Beijing, China. He became an Assistant Professor in 2016, an Associate Professor in 2018, a Professor in 2022, and then Academic Associate Dean with the school of mechanical engineering, Zhejiang Sci-Tech University. In 2017, he was a Visiting Scholar with Virginia Tech, Blacksburg, VA, USA. He has been funded by 4 NSFCs including Excellent Young Scientist Fund. He has authored more than 60 peer-reviewed journal articles. His research interests include nonlinear vibration and control, bio-inspired vibration structure, and dynamics of high-end equipment.

Li Cheng received the B.S. degree from Xi'an Jiaotong University, China, and the Ph.D. degree from the Institute National des Sciences Appliques de Lyon, France.

He is now a Chair Professor at The Hong Kong Polytechnic University. His research focuses on sound and vibration, structural health monitoring, and smart structure and control

He is a Fellow of the Royal Society of Canada (Academy of Science), a Fellow of the Canadian Academy of Engineering, and a Distinguished Fellow of the International Institute of Acoustics and Vibration. He is Deputy Editor-in-Chief of Journal of Sound and Vibration, Associate Editor of Journal of the Acoustical Society of America, Associate Editor of Structural Health Monitoring: An International Journal, and Topical Associate Editor of Nonlinear Dynamics.